

NOTE TO USERS

PREVIEW

This reproduction is the best copy available.

UMI[®]

PREVIEW

CHARACTERIZING SCALE-DEPENDENT SPATIAL STRUCTURE IN MULTI-RESOLUTION,
MULTI-TEMPORAL AND HYPERSPECTRAL REMOTELY SENSED IMAGERY

by

Weirong Chen

A DISSERTATION

Presented to the Faculty of
The Graduate College at the University of Nebraska
In Partial Fulfillment of Requirements
For the Degree of Doctor of Philosophy

Major: Geography

Under the Supervision of Professor Geoffrey M. Henebry

Lincoln, Nebraska

October 2004

UMI Number: 3149623

INFORMATION TO USERS

The quality of this reproduction is dependent upon the quality of the copy submitted. Broken or indistinct print, colored or poor quality illustrations and photographs, print bleed-through, substandard margins, and improper alignment can adversely affect reproduction.

In the unlikely event that the author did not send a complete manuscript and there are missing pages, these will be noted. Also, if unauthorized copyright material had to be removed, a note will indicate the deletion.

UMI[®]

UMI Microform 3149623

Copyright 2005 by ProQuest Information and Learning Company.

All rights reserved. This microform edition is protected against unauthorized copying under Title 17, United States Code.

ProQuest Information and Learning Company
300 North Zeeb Road
P.O. Box 1346
Ann Arbor, MI 48106-1346

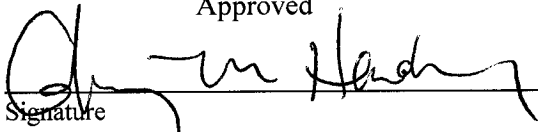
DISSERTATION TITLE

Characterizing scale-dependent spatial structure in multi-resolution, multi-temporal and
hyperspectral remotely sensed imagery

BY


Weirong Chen

SUPERVISORY COMMITTEE:

Approved

Signature

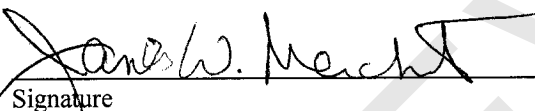
Geoffrey M. Henebry
Typed Name

Date
14 OCT 04


Signature

Donald C. Rundquist
Typed Name

14 OCT 04


Signature


James W. Merchant
Typed Name

14 Oct. 04


Signature

Stephen J. Lavin
Typed Name

14 Oct. 04


Signature

Stephen E. Reichenbach
Typed Name

14 Oct 04

Signature

Typed Name

UNIVERSITY OF
Nebraska
Lincoln

CHARACTERIZING SCALE-DEPENDENT SPATIAL STRUCTURE IN MULTI-RESOLUTION,
MULTI-TEMPORAL AND HYPERSPECTRAL REMOTELY SENSED IMAGERY

Weirong Chen, Ph.D.

University of Nebraska, 2004

Advisor: Geoffrey M. Henebry

Spatial structure information characterized from remotely sensed imagery can be used in various applications. Previous studies in this field were mostly concentrated on forests, grasslands or wetlands. Little attention was paid to the crop canopies, where this information is needed for remote sensing of agriculture. In this research, the scale-dependent spatial structure in remotely sensed imagery from different sources acquired over agricultural crop canopies was characterized to assess the effect on observed spatial structure stemming from changes in spatial, spectral and temporal factors. Three research questions were addressed: (1) What is the effect of spatial resolution on observed spatial structure and how good is the correspondence between measured and rescaled data sets? (2) How does the temporal development of spatial structure differ among spectral wavebands and indices? (3) How does observed spatial structure change with spectral resolution and wavelength? The study was conducted at the University of Nebraska Agricultural Research and Development Center, near Mead, Nebraska. Spatial structure characterization was carried out using lacunarity, semivariogram, and scale of fluctuation analyses. Results indicated that: (1) Due to the difference in spatial structure of fractional

vegetation cover (FVC), one crop FVC has higher lacunarity and more complicated lacunarity deviation than the other. (2) Regularization can lead to the decrease in amount of spatial variability and increase in spatial dependence, and rescaling via block averaging can overly retain original spatial structure, which may be reduced via spatial filtering operations prior to rescaling. (3) Spatio-temporal patterns are different between vegetation indices and their component bands, and vegetation indices are more sensitive to the development of crop canopies than their component bands. (4) The degree of spatial variation with wavelength is correlated to the degree of the difference in reflectance of underlying targets and increasing bandwidth may blur spatial structure that occurs at finer spectral resolution. These findings are useful for studies of rescaling, crop monitoring, sampling design, and identification of an appropriate spatial resolution for agricultural remote sensing.

PREVIEW

ACKNOWLEDGEMENTS

I wish to thank my advisor Dr. Geoff Henebry for his support, both academic and financial, without which I would not have finished this dissertation. Dr. Henebry spent a lot of time on this dissertation and provided me numerous constructive suggestions, which ultimately helped to define the general structure of the dissertation.

I wish to thank Dr. Donald Rundquist, who provided me assistantship and gave me the opportunity to study in the Center of Advanced Land Management Information Technologies (CALMIT). As a former chair of my committee, Dr. Rundquist helped me to form the committee and define the courses for my Ph. D. program. As a reader of the dissertation, he provided me a lot of detailed suggestions to get the dissertation improved considerably.

I wish to thank Dr. James Merchant, who agreed to be my committee member and a reader of the dissertation. This dissertation benefited a lot from his multitude of comments and suggestions.

I also wish to thank Drs. Steve Lavin and Steve Reichenbach, who agreed to be my committee members and spent their precious time throughout the different stages of my Ph. D. study.

Finally, I would like to thank all other faculty, staff and students in CAMLIT for their various helps during my stay in CALMIT. I feel lucky and am honored for once being a member of CALMIT.

TABLE OF CONTENTS

Chapter 1 Introduction.....	1
References.....	6
Chapter 2 Background and literature review.....	11
2.1 Introduction.....	11
2.2 Semivariogram analysis.....	12
2.3 Lacunarity analysis.....	15
2.4 Scale of fluctuation analysis.....	17
2.5 Summary and comments.....	20
References.....	22
Chapter 3 Examining scale-dependent spatial structure of fractional vegetation cover using lacunarity analysis.....	27
3.1 Introduction.....	27
3.2 Methods.....	28
3.2.1 Lacunarity, neutral model and percent deviations.....	28
3.2.2 Study area and data collection.....	31
3.2.3 Image extraction, FVC image formation, and lacunarity and its percent deviation computation.....	32
3.3 Results.....	33
3.4 Discussion.....	35
3.4.1 Effects of crop type on FVC spatial structure	35
3.4.2 Effects of spatial resolution on FVC spatial structure	37

3.5 Conclusion.....	38
References.....	40
Chapter 4 Analyzing the change of spatial information under rescaling: a case study using multi-resolution aerial data	
4.1 Introduction.....	69
4.2 Methods.....	70
4.2.1 Study area, imagery acquisition, and preprocessing.....	70
4.2.2 Image extraction, rescaling and semivariance computation.....	72
4.3 Results.....	73
4.4 Discussion.....	75
4.5 Conclusion.....	79
References.....	80
Chapter 5 Seasonal spatial structure analysis of corn and soybean canopy using multi-date high resolution aircraft imagery.....	
5.1 Introduction.....	91
5.2 Methods.....	92
5.2.1 Study area, crop description, image acquisition and preprocessing.....	93
5.2.2 Image subset, semivariance and correlation length computation.....	93
5.3 Results	94
5.4 Discussion	96

5.5 Conclusion.....	99
References.....	102
Chapter 6 Spatio-spectral heterogeneity analysis using EO-1 hyperion imagery.....	131
6.1 Introduction.....	131
6.2 Methods.....	133
6.2.1 Study area, imagery acquisition and preprocessing.....	133
6.2.2 Semivariance and correlation length computation.....	134
6.3 Results and discussion.....	135
6.4 Conclusion.....	139
References.....	142
Chapter 7 Concluding remarks.....	149

PREVIEW

LIST OF TABLES

Table 3.1	Fractional vegetation cover (in percentage) for soybean plots.....	43
Table 3.2	Fractional vegetation cover (in percentage) for sorghum plots.....	43
Table 3.3	Statistical test results for soybeans.....	44
Table 3.4	Statistical test results for sorghum.....	45
Table 4.1	Descriptive statistics for the observed and rescaled image series.....	83
Table 4.2	Sill+nugget variance ($c+c_0$) and range (a_0) parameters in models fit to transect data for observed and rescaled image series.....	84
Table 4.3	Percent change from the lowest altitude (finest spatial resolution) of sill+nugget variance ($c+c_0$) and range (a_0) parameters in models fit to transect data for observed and rescaled image series.....	85
Table 4.4	The variation in sill+nugget variance ($c+c_0$) and range (a_0) as the finest observed data (0.187m) were successively smoothed using a low-pass 3x3 filter before being rescaled to the next coarser spatial resolution (0.373m).....	86
Table 5.1	Description of crop growth stages when data were acquired.....	106

LIST OF FIGURES

Figure 2.1	A typical spherical model of semivariogram.....	13
Figure 2.2	Three typical lacunarity decay patterns	16
Figure 2.3	(A) Normalized variance as function of window sizes; (B) Scales of fluctuation as function of window sizes.....	18
Figure 3.1	Image samples for soybeans acquired from different heights. All presented in R(red) and G(NIR) combination. Numbers indicate the acquisition heights.....	46
Figure 3.2	Image samples for sorghum acquired from different heights. All presented in R(red) and G(NIR) combination. Numbers indicate the acquisition heights.....	47
Figure 3.3	Map of fractional vegetation cover for soybeans derived from Plot A at four heights. Numbers indicate the acquisition heights (first) and spatial resolution (second) respectively. Vegetation is displayed in gray color.....	48
Figure 3.4	Map of fractional vegetation cover for soybeans derived from Plot B at four heights. Numbers indicate the acquisition heights (first) and spatial resolution (second) respectively. Vegetation is displayed in gray color.....	49
Figure 3.5	Map of fractional vegetation cover for soybeans derived from Plot C at	

	four heights. Numbers indicate the acquisition heights (first) and spatial resolution (second) respectively. Vegetation is displayed in gray color.....	50
Figure 3.6	Map of fractional vegetation cover for soybeans derived from Plot D at four heights. Numbers indicate the acquisition heights (first) and spatial resolution (second) respectively. Vegetation is displayed in gray color.....	51
Figure 3.7	Map of fractional vegetation cover for soybeans derived from Plot E at four heights. Numbers indicate the acquisition heights (first) and spatial resolution (second) respectively. Vegetation is displayed in gray color.....	52
Figure 3.8	Map of fractional vegetation cover for sorghum derived from Plot A at four heights. Numbers indicate the acquisition heights (first) and spatial resolution (second) respectively. Vegetation is displayed in gray color.....	53
Figure 3.9	Map of fractional vegetation cover for sorghum derived from Plot B at four heights. Numbers indicate the acquisition heights (first) and spatial resolution (second) respectively. Vegetation is displayed in gray color.....	54
Figure 3.10	Map of fractional vegetation cover for sorghum derived from Plot C at four heights. Numbers indicate the acquisition heights (first) and spatial resolution (second) respectively. Vegetation is displayed in gray color.....	55

- Figure 3.11 Map of fractional vegetation cover for sorghum derived from Plot D at four heights. Numbers indicate the acquisition heights (first) and spatial resolution (second) respectively. Vegetation is displayed in gray color.....56
- Figure 3.12 Map of fractional vegetation cover for sorghum derived from Plot E at four heights. Numbers indicate the acquisition heights (first) and spatial resolution (second) respectively. Vegetation is displayed in gray color.....57
- Figure 3.13 Plot A of soybeans. Different symbols are for different spatial resolutions: solid circle = 0.248cm, open square = 0.456cm, solid square = 0.664, open circle = 0.872cm. (I) Lacunarity function of the FVC slice. (II) FVC percent lacunarity index deviation vs. window size at varying spatial resolutions. Dashed line stands for the perfect self-similar situation. (III) Logarithm of lacunarity index vs. its deviation at varying spatial resolutions. Numbers stand for the three sampling window sizes used: 1 = 10cm; 2 = 35cm; 3 = 60cm.....58
- Figure 3.14 Plot B of soybeans. Different symbols are for different spatial resolutions: solid circle = 0.231cm, open square = 0.439cm, solid square = 0.647cm, open circle = 0.855cm. (I) Lacunarity function of the FVC slice. (II) FVC percent lacunarity index deviation vs. window size at varying spatial resolutions. (III) Logarithm of lacunarity index vs. its deviation at varying spatial resolutions. Numbers stand for the three sampling window sizes used: 1 = 10cm; 2 = 33cm; 3 = 56cm.....59

- Figure 3.15 Plot C of soybeans. Different symbols are for different spatial resolutions:
solid circle = 0.245cm, open square = 0.453cm, solid square = 0.661cm,
open circle = 0.869cm. (I) Lacunarity function of the FVC slice. (II) FVC
percent lacunarity index deviation vs. window size at varying spatial
resolutions. (III) Logarithm of lacunarity index vs. its deviation at varying
spatial resolutions. Numbers stand for the three sampling window sizes
used: 1 = 10cm; 2 = 35cm; 3 = 59cm.....60
- Figure 3.16 Plot D of soybeans. Different symbols are for different spatial resolutions:
solid circle = 0.274cm, open square = 0.482cm, solid square = 0.690cm,
open circle = 0.898cm. (I) Lacunarity function of the FVC slice. (II) FVC
percent lacunarity index deviation vs. window size at varying spatial
resolutions. (III) Logarithm of lacunarity index vs. its deviation at varying
spatial resolutions. Numbers stand for the three sampling window sizes
used: 1 = 12cm; 2 = 39cm; 3 = 64cm.....61
- Figure 3.17 Plot E of soybeans. Different symbols are for different spatial resolutions:
solid circle = 0.266cm, open square = 0.473cm, solid square = 0.681cm,
open circle = 0.889cm. (I) Lacunarity function of the FVC slice. (II) FVC
percent lacunarity index deviation vs. window size at varying spatial
resolutions. (III) Logarithm of lacunarity index vs. its deviation at varying
spatial resolutions. Numbers stand for the three sampling window sizes
used: 1 = 13cm; 2 = 39cm; 3 = 64cm.....62
- Figure 3.18 Plot A of sorghum. Different symbols are for different spatial resolutions:

solid circle = 0.208cm, open square = 0.416cm, solid square = 0.624cm, open circle = 0.831cm. (I) Lacunarity function of the FVC slice. (II) FVC percent lacunarity index deviation vs. window size at varying spatial resolutions. (III) Logarithm of lacunarity index vs. its deviation at varying spatial resolutions. Numbers stand for the three sampling window sizes used: 1 = 8.5cm; 2 = 29cm; 3 = 50cm.....63

Figure 3.19 Plot B of sorghum. Different symbols are for different spatial resolutions: solid circle = 0.208cm, open square = 0.416cm, solid square = 0.624cm, open circle = 0.831cm. (I) Lacunarity function of the FVC slice. (II) FVC percent lacunarity index deviation vs. window size at varying spatial resolutions. (III) Logarithm of lacunarity index vs. its deviation at varying spatial resolutions. Numbers stand for the three sampling window sizes used: 1 = 8.5cm; 2 = 29cm; 3 = 50cm.....64

Figure 3.20 Plot C of sorghum. Different symbols are for different spatial resolutions: solid circle = 0.208cm, open square = 0.416cm, solid square = 0.624cm, open circle = 0.831cm. (I) Lacunarity function of the FVC slice. (II) FVC percent lacunarity index deviation vs. window size at varying spatial resolutions. (III) Logarithm of lacunarity index vs. its deviation at varying spatial resolutions. Numbers stand for the three sampling window sizes used: 1 = 8.5cm; 2 = 29cm; 3 = 50cm.....65

Figure 3.21 Plot D of sorghum. Different symbols are for different spatial resolutions: solid circle = 0.208cm, open square = 0.416cm, solid square = 0.624cm,

- open circle = 0.831cm. (I) Lacunarity function of the FVC slice. (II) FVC percent lacunarity index deviation vs. window size at varying spatial resolutions. (III) Logarithm of lacunarity index vs. its deviation at varying spatial resolutions. Numbers stand for the three sampling window sizes used: 1 = 8.5cm; 2 = 29cm; 3 = 50cm.....66
- Figure 3.22 Plot E of sorghum. Different symbols are for different spatial resolutions: solid circle = 0.208cm, open square = 0.416cm, solid square = 0.624cm, open circle = 0.831cm. (I) Lacunarity function of the FVC slice. (II) FVC percent lacunarity index deviation vs. window size at varying spatial resolutions. (III) Logarithm of lacunarity index vs. its deviation at varying spatial resolutions. Numbers stand for the three sampling window sizes used: 1 = 8.5cm; 2 = 29cm; 3 = 50cm.....67
- Figure 3.23 Simulated images. Symbols are for the same spatial resolutions as the crops. (I) Averaged lacunarity functions derived from a series of simulated random images based on the crop plot dimensions. (II) Averaged percent lacunarity index deviation vs. window size for simulated images.....68
- Figure 4.1 Semivariograms derived from the observed image series. Solid square is for 0.187m, solid circle for 0.388m, and open square for 1m.....87
- Figure 4.2 Semivariograms derived from the rescaled image series. Solid square is for 0.187m, solid circle for 0.373m, and open square for 0.933m.....88
- Figure 4.3 Plots of the ratio of the sill+nugget variance ($c+c_0$) to the range (a_0) against the natural logarithm of the areal resolution for the observed

	and rescaled data sets. Open square is for the observed and solid circle is for the rescaled. Numbers and letters indicate resolution levels for the observed and the rescaled, respectively: 0 = 0.187m; 1 = 0.388m; 2 = 1m; a = 0.373m; c = 0.933m.....	89
Figure 4.4	Plots of the sill+nugget variance ($c+c_0$) against the range (a_0) for the finest observed data that were first smoothed using a 3 x 3 low-pass filter before being rescaled to the next coarser spatial resolution (0.373m). Numbers indicate the times of the smoothing operations performed before rescaling. The parameters of the observed images at 0.388m were also illustrated (solid circle).....	90
Figure 5.1	Images of NIR band for corn and soybeans acquired on three different dates.....	107
Figure 5.2	Images of red band for corn and soybeans acquired on three different dates.....	108
Figure 5.3	Images of green band for corn and soybeans acquired on three different dates.....	109
Figure 5.4	NDVI images for corn and soybeans derived from three different dates.....	110
Figure 5.5	GNDVI images for corn and soybeans derived from three different dates.....	111
Figure 5.6	Semivariograms derived from NIR band over corn crop. (a) west-east direction; (b) north-south direction. Diamond is for June 22, square for	

	July 7, and triangle for August 26.....	112
Figure 5.7	Semivariograms derived from red band over corn crop. (a) west-east direction; (b) north-south direction. Diamond is for June 22, square for July 7, and triangle for August 26.....	113
Figure 5.8	Semivariograms derived from green band over corn crop. (a) west-east direction; (b) north-south direction. Diamond is for June 22, square for July 7, and triangle for August 26.....	114
Figure 5.9	Semivariograms derived from NDVI images over corn crop. (a) west-east direction; (b) north-south direction. Diamond is for June 22, square for July 7, and triangle for August 26.....	115
Figure 5.10	Semivariograms derived from GNDVI images over corn crop. (a) west-east direction; (b) north-south direction. Diamond is for June 22, square for July 7, and triangle for August 26.....	116
Figure 5.11	Semivariograms derived from NIR band over soybean crop. (a) west-east direction; (b) north-south direction. Diamond is for June 22, square for July 7, and triangle for August 26.....	117
Figure 5.12	Semivariograms derived from red band over soybean crop. (a) west-east direction; (b) north-south direction. Diamond is for June 22, square for July 7, and triangle for August 26.....	118
Figure 5.13	Semivariograms derived from green band over soybean crop. (a) west-east direction; (b) north-south direction. Diamond is for June 22, square for July 7, and triangle for August 26.....	119

Figure 5.14	Semivariograms derived from NDVI images over soybean crop. (a) west-east direction; (b) north-south direction. Diamond is for June 22, square for July 7, and triangle for August 26.....	120
Figure 5.15	Semivariograms derived from GNDVI images over soybean crop. (a) west-east direction; (b) north-south direction. Diamond is for June 22, square for July 7, and triangle for August 26.....	121
Figure 5.16	Sill+nugget variance of NIR, red and green band against GDD after planting for corn (open) and soybeans (solid). Square (diamond) = west-east (north-south) direction.....	122
Figure 5.17	Sill+nugget variance of NDVI and GNDVI against GDD after planting for corn (open) and soybeans (solid). Square (diamond) = west-east (north-south) direction.....	123
Figure 5.18	Range values of NIR, red and green band against GDD after planting for corn (open) and soybeans (solid). Square (diamond) = west-east (north-south) direction.....	124
Figure 5.19	Range values of NDVI and GNDVI against GDD after planting for corn (open) and soybeans (solid). Square (diamond) = west-east (north-south) direction.....	125
Figure 5.20	Correlation lengths of NIR, red, and green band against GDD after planting for corn (open) and soybeans (solid). The extensions above and below the diamonds represent $\pm 2^*$ standard error.....	126
Figure 5.21	Correlation lengths of NDVI and GNDVI against GDD after planting for	

	corn (open) and soybeans (solid). The extensions above and below the diamonds represent $\pm 2 \times$ standard error.....	127
Figure 5.22	Mean reflectances of NIR, red and green band against GDD after planting for corn (open) and soybeans (solid). The extensions above and below the symbols represent $\pm 2 \times \delta$ (standard deviation).....	128
Figure 5.23	Mean indices of NDVI and GNDVI against GDD after planting for corn (open) and soybeans (solid). The extensions above and below the symbols represent $\pm 2 \times \delta$ (standard deviation).....	129
Figure 5.24	Typical ground shots for (a) soybean and (b) corn crops on June 22, 2000.....	130
Figure 6.1	Location and extent of ARDC and a sum image of all bands selected for the study. Dashed rectangle stands for the area covered by the data actually used in the study.....	144
Figure 6.2	Sill+nugget variance ($c+c_0$) as a function of wavelength. Open triangle (square) is for the north-south (west-east) direction; filled circle is for the %CV of reflectance of the entire image. Dashed vertical lines and horizontal gray bars show the placement of Landsat TM/ETM+ bands, whose sill+nugget variances are shown as the large solid triangle (north-south) and large open square (west-east).....	145
Figure 6.3	The percent difference in reflectance between soil and green vegetation (open circle) and the %CV of reflectance of the entire image (filled circle) as a function of wavelength. Dashed line indicates no difference in reflectance between soil and green vegetation.....	146

- Figure 6.4 Range as a function of wavelength. Open triangle (square) is for the north-south (west-east) direction, and filled circle is for the %CV of reflectance of the entire image. Dashed lines and gray bars represent the width of Landsat TM/ETM+ bands, whose corresponding ranges are shown as the large solid triangle (north-south) and square (west-east).....147
- Figure 6.5 The effect of wavelength on the correlation length. Open triangle is for correlation length, filled circle is for %CV of reflectance of the entire image, and open circle is for %CV of reflectance via random walk sampling. Dashed lines and gray bars represent the width of Landsat TM/ETM+ bands, whose corresponding correlation lengths are shown as the large solid triangle.....148

PREVIEW

CHAPTER 1

INTRODUCTION

Remote sensing has become an important tool for mapping and monitoring vegetation cover (Hobbs, 1990; Mantovani and Setzer, 1997; Young and Wang, 2001). The majority of the research work to date has concentrated on the spectral properties of the data. In contrast, the spatial domain has received considerably less attention in image analysis. Spatial domain is an important aspect of remotely sensed imagery and contains lots of useful information. Estes et al. (1983) included size, shape, texture, height, shadow, site, and association, all as inherent elements within an image that can provide an image analyst clues for interpretation. Many studies have also shown that texture is useful to improve image classification (Haralick and Shanmugam, 1973; Agbu and Nizeyimana, 1991; Barber and LeDrew, 1991; Peddle and Franklin, 1991).

Spatial pattern can be generally defined as the amount and variability of a system property in space and time (Davidson and Csillag, 2003). Spatial structure is a subset of the concept of spatial pattern and refers to the spatial components of heterogeneity (i.e., the way in which total landscape variability is partitioned across spatial scales) (Gustafson, 1998). Originally used in ecological studies, spatial structure in remote sensing pays more attention to the overall spatial arrangement of pixels across the entire image. This is different from texture, which emphasizes more on tonal repetitions within an object, or within groups of objects that are too small to be discerned individually.